

Preliminary airborne measurement results from the Hyperspectral Polarimeter for Aerosol Retrievals (HySPAR).

Stephen H. Jones, Frank J. Iannarilli, Chris Hostetler, Brian Cairns, Anthony Cook, John Hair, David Harper, Yongxiang Hu, and David Flittner

Abstract—The Hyperspectral Polarimeter for Aerosol Retrievals (HySPAR) acquires a 120 degree spatial, full-Stokes (i.e. including V) line image over 480-960 nm in a single snapshot with no moving parts. Unlike other snapshot polarimeters that typically use multiple boresighted beams or micro-polarizer pixel masks, HySPAR uses an arrangement of birefringent crystals to impart a polarization dependent modulation on the measured spectrum. The modulated spectra can be inverted to yield Stokes spectra. Preliminary airborne measurement results from the Megacity Initiative: Local and Global Research Observations (MILAGRO) campaign will be presented. HySPAR Stokes imagery will be compared to that of the Research Scanning Polarimeter (RSP). These data were acquired during coordinated flight paths of the two aircraft carrying the sensors.

Index Terms—Polarimetry, spectropolarimetry, aerosol.

I. INTRODUCTION

THE Hyperspectral Polarimeter for Aerosole Retrievals (HySPAR) is based on a technique for simultaneously measuring perfectly registered spectra and full Stokes polarization state on a single focal plane array, in a single integration period. The technique, Polarimetric Spectral Intensity Modulation (PSIM)¹, modulates the spectrum in a polarization dependent manner, using birefringent crystals. The full Stokes vector can subsequently be retrieved from the spectrum. In a single integration period, the focal plane records one dimension of spatial information (columns) and one dimension of modulated spectra (rows) as shown in Figure 1. The only moving part is a shutter that controls the exposure time. The technology is innovative in the sense that all other existing sensors perform spectropolarimetry by multiplexing in time (e.g. rotating polarizer/waveplate implementations) or multiplexing in space (e.g. subpixel polarization masks, multiple boresighted sensors).

It is important to observe and characterize natural and anthropogenic tropospheric aerosols because of 1) their contribution to the radiation budget and, hence, their climate forcing effect, 2) the future cleansing capacity of the atmosphere, and

S. J. Jones and F. J. Iannarilli are with Aerodyne Research, Inc., 45 Manning Rd., Billerica, MA 01821 (sjones@aerodyne.com).

C. Hostetler, A. Cook, J. Hair, D. Harper, Y. Hu, and D. Flittner are with the Climate Science Branch, Science Directorate, NASA Langley Research Center, Hampton, VA, 23681.

B. Cairns is with the Department of Applied Physics and Applied Mathematics, Columbia University, New York, NY 10025.

¹U.S. Patent 6,490,043, P. Kebabian, "Polarimetric spectral intensity modulation spectropolarimeter".

3) the role of atmospheric chemistry in changing the composition of aerosols that affect human health, the environment, visibility, and infrastructural materials[1]. The PSIM technique is particularly relevant to NASA's efforts to quantify the parameters of tropospheric aerosols by remotely sensing their radiative properties and integrated column effect. Furthermore, more accurate retrieval of aerosol properties will improve the ability to correct other remotely sensed data for the effects of scattering and absorption. It has been shown that polarization and view angle diversity are powerful sensing modalities for the retrieval of aerosol properties[2][3]. It has also been observed that

Technologies such as scanning polarimeters in the visible and near infrared appear able to retrieve tropospheric aerosol scattering characteristics from measurements of multispectral radiance and polarization by resolving aerosols from clouds and thus hold promise[1].

Aerodyne has demonstrated the PSIM technique in the laboratory at both VIS and LWIR wavelengths[4], in ground-based field experiments and, as described here, in an airborne setting. An example PSIM spectrum from the laboratory demonstration is shown in Figure 1. The incident light was essentially 100% polarized. Note the 0 and 90 degree cases are of opposite phase. The modulation effect is sinusoidal in *wavenumber*, hence the chirped appearance in wavelength. The 45 and 135 degree cases contain other frequency components, as can be seen from the shallower nulls at the some wavelengths. It is shown in the text how the spectrum can be demodulated to retrieve the full Stokes polarization state.

The specific benefits offered by HySPAR can be summarized as follows:

- Perfectly registered, simultaneously acquired spectrum and polarimetry.
- Single snapshot polarimetry.
- No moving parts other than a shutter.
- Imaging capability.
- Simple, rugged optical system
- Potential to retrofit an existing hyperspectral imager.

In the following sections we give a brief description of the HySPAR sensor followed by field results from MILAGRO. The results include comparison of HySPAR data with those simultaneously acquired by the Research Scanning Polarimeter (RSP)[5]. RSP, also a *spectropolarimeter*, is based on multiple

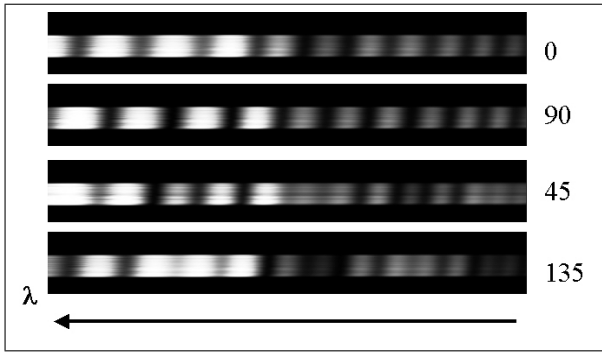


Fig. 1. Sample raw data from original PSIM lab prototype taken at various angles of polarization.

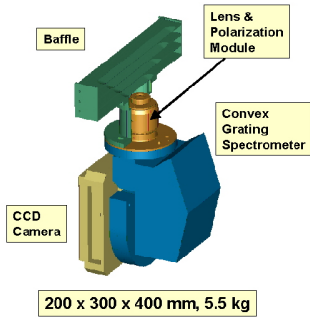


Fig. 2. Schematic representation of HySPAR with baffle partially cut away to show location and size of lens.

boresighted telescopes and a mechanical scanning mechanism. This design achieves temporal simultaneity by generating multiple beams, spectrally via dichroic filters, and polarimetrically via polarizing beamsplitters.

II. HYSPAR INSTRUMENT

A. Overview

HySPAR employs a novel configuration of two *stationary* birefringent crystals, followed by a *stationary* polarizer, packaged in a *polarization module*. When placed optically upstream from the spectrometer dispersing element this polarization module induces polarization-dependent interference fringes upon the measured intensity spectrum. There are no moving parts other than the detector shutter. The full Stokes vector spectrum can subsequently be retrieved from the modulated intensity spectrum, based on the fringe patterns. In a single integration period, the focal plane in the slit-based line-imaging spectrometer records spatial information along one dimension (columns) and modulated spectra along the other dimension (rows).

Figure 2 shows a schematic representation of HySPAR with the baffle partially cut away to show the size and location of the lens. Figure 3 shows the layout of the optical components in the lens. The polarization module is located in

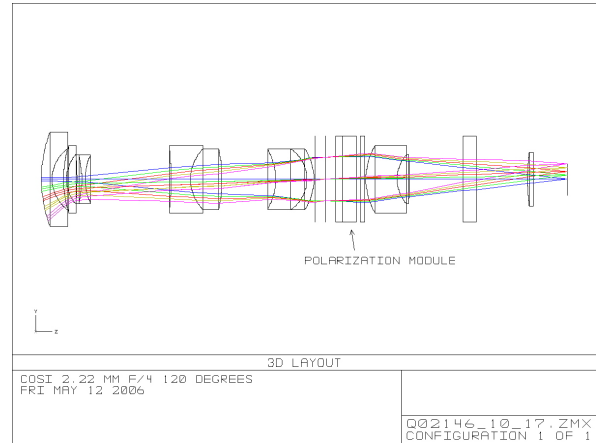


Fig. 3. Schematic layout of the HySPAR optical system. The polarization module, consisting of two stationary retarders and a stationary polarizer, is located in a nearly collimated region within the lens. Angles of incidence are less than 5 degrees throughout the polarization sensitive portion of the system to maintain low diattenuation.

a nearly collimated region of the beam to insure near normal incidence at the crystals for all rays. All angles of incidence forward of the stationary polarizer, the last element in the polarization module, are less than five degrees to minimize "self-polarization" effects. The image formed by the lens is telecentric for a proper interface to the convex grating spectrometer.

B. Mueller Matrix Representation

The Mueller calculus is a convenient means of describing the polarization state of a single beam of light as it propagates through a system [6]. The system Mueller matrix describing on-axis propagation through the PSIM polarization module is simply

$$\mathbf{M}_{sys} = \mathbf{M}_{pol} \cdot \mathbf{M}_{crystal2} \cdot \mathbf{M}_{crystal1} \quad (1)$$

which is evaluated using standard forms for the component matrices. However, since the photon detector measures only intensity, only the first row of \mathbf{M}_{sys} is relevant for describing the detected spectral intensity $I(\nu)$:

$$\begin{aligned} I(\nu) &= \mathbf{m}_{sys,1}(\nu) \cdot \mathbf{s}(\nu) \\ &= \frac{1}{4} \begin{bmatrix} 2 \\ 2 \cos \phi_2 \\ \cos \Delta\phi - \cos \Sigma\phi \\ \sin \Sigma\phi - \sin \Delta\phi \end{bmatrix}^T \cdot \begin{bmatrix} s_0 \\ s_1 \\ s_2 \\ s_3 \end{bmatrix} \end{aligned} \quad (2)$$

where,

ν	=	Optical frequency (Hz)
c	=	Speed of Light
$I(\nu)$	=	Detected spectral intensity
$\mathbf{m}_{sys,1}(\nu)$	=	First row of system Mueller matrix, \mathbf{M}_{sys}
$\mathbf{s}(\nu)$	=	Incident Stokes vector
$\Delta\phi$	=	$\phi_1 - \phi_2$
$\Sigma\phi$	=	$\phi_1 + \phi_2$
ϕ_1	=	$2\pi\nu(n_e - n_o)\ell_1/c$
ϕ_2	=	$2\pi\nu(n_e - n_o)\ell_2/c$
n_o, n_e	=	Crystal indices of refraction
ℓ_1, ℓ_2	=	Crystal lengths.

and presuming our canonical crystal and polarizer orientations. Equation (2) is valid for an infinitesimal frequency band. Since a pixel represents a finite band and the point spread function also has finite extent, (2) must be multiplied by a blur kernel that characterizes the point spread function and then integrated over the significant region of support of the blur kernel.

C. Linear-Spectrum Signal Model and Stokes Inversion

The linear-spectrum model is motivated by the failure of the *constant-spectrum* model which, when employed against sources exhibiting even modest spectral variation such as a linear trend, induces objectionable ripple artifacts in the inverted Stokes spectrum. In this section we describe the salient aspects of the model and its inversion. A more complete description, including calibration issues, is discussed in [4]. The forward model for the PSIM-modulated data, \mathbf{d} , within a spectral analysis window centered at pixel x_o is:

$$\mathbf{d} = \mathbf{M}_1(x_o, y_o) \mathbf{s}_1(x_o, y_o) \quad (3)$$

where \mathbf{d} is a data vector of length $2N + 1$ spectral samples. $\mathbf{M}_1(x_o, y_o)$ is the forward system matrix for the spectral samples centered about pixel (x_o, y_o) , and $\mathbf{s}_1(x_o, y_o)$ is the incident Stokes vector for wavelength $\lambda(x_o, y_o)$ at the *center* of the pixel. The linear-spectrum model assumes that $\mathbf{s}_1(x_o, y_o)$ exhibits linear variation with wavelength *within* a $2N + 1$ sample-length analysis window. An inversion can be performed at each pixel, yielding a smoothing effect similar to a boxcar moving average filter with an impulse response of the same extent as the PSIM analysis window. Thus, although an inversion is computed at each pixel, the effective resolution is on the order of the window length.

Within an analysis window, the incident Stokes spectrum $\mathbf{s}(x - x_o)$ is presumed to exhibit linear dependence on wavelength, expressed by a spectral constant (pedestal) and a spectral linear ramp signal for each Stokes component:

$$\mathbf{s}(x - x_o) = \begin{bmatrix} I_0 + I_1(x - x_o) \\ Q_0 + Q_1(x - x_o) \\ U_0 + U_1(x - x_o) \\ V_0 + V_1(x - x_o) \end{bmatrix} \quad (4)$$

where x is the continuous wavelength variable normalized in pixel units. For modeling purposes, we stack the coefficients of the above Stokes linear spectrum model into an *augmented* Stokes vector:

$$\mathbf{s}_1(x_o, y_o) = [I_0 \quad Q_0 \quad U_0 \quad V_0 \quad I_1 \quad Q_1 \quad U_1 \quad V_1]^T. \quad (5)$$

The corresponding system matrix is:

$$\mathbf{M}_1(\delta; x_o, y_o) = \begin{bmatrix} \mathbf{m}_0(x_o - N, y_o) & \mathbf{m}_1(x_o - N, y_o) \\ \vdots & \vdots \\ \mathbf{m}_0(x_o - 1, y_o) & \mathbf{m}_1(x_o - 1, y_o) \\ \mathbf{m}_0(x_o, y_o) & \mathbf{m}_1(x_o, y_o) \\ \mathbf{m}_0(x_o + 1, y_o) & \mathbf{m}_1(x_o + 1, y_o) \\ \vdots & \vdots \\ \mathbf{m}_0(x_o + N, y_o) & \mathbf{m}_1(x_o + N, y_o) \end{bmatrix} \quad (6)$$

where

$$\mathbf{m}_p(x_o + i, y_o) = \begin{bmatrix} m_{Ip}(x_o + i, y_o) \\ m_{Qp}(x_o + i, y_o) \\ m_{Up}(x_o + i, y_o) \\ m_{Vp}(x_o + i, y_o) \end{bmatrix}^T \quad (7)$$

and x_o is the FPA detector index in dispersion dimension (indexing wavelength), i is the relative pixel index within analysis window: $i \in [-N, N]$ and y_o is the pixel index along the spatial (slit) dimension. The matrix elements of (7) correspond to the system model functions of order p . For instance, \mathbf{m}_0 is given by (2) and \mathbf{m}_1 corresponds to the linear model functions.

With $N \geq 4$, the linear-spectrum forward model of (3) and (6) forms an overdetermined system that we invert in a least squares sense using the pseudoinverse $\mathbf{M}_1^+(x_o, y_o)$, which results from the singular value decomposition of \mathbf{M}_1 . The system matrix for a properly designed instrument is always well conditioned so all singular values are retained in the inversion.

The inverted augmented Stokes vector corresponding to the data is computed as follows:

$$\widehat{\mathbf{s}}_1(x_o, y_o) = \mathbf{M}_1^+(x_o, y_o) \mathbf{d}. \quad (8)$$

We report the Stokes vector for the analysis window as:

$$\widehat{\mathbf{s}} = [\widehat{I}_0 \quad \widehat{Q}_0 \quad \widehat{U}_0 \quad \widehat{V}_0]. \quad (9)$$

That is, we report the scalar intensities of the spectrally-constant Stokes signal terms. The values of $\widehat{I}_1, \widehat{Q}_1$, etc. represent the slopes of the linear ramp terms $(x - x_o)$. These slope values are presently discarded. Since the linear ramp atoms are zero-mean over the analysis window, $[\widehat{I}_0 \quad \widehat{Q}_0 \quad \widehat{U}_0 \quad \widehat{V}_0]$ thus represents the mean value of the Stokes vector within the analysis window.

III. RESULTS

The data presented in this section were acquired as part of the MILAGRO measurement campaign that took place during March 2006. MILAGRO consisted of four simultaneous measurement campaigns, each focusing on somewhat different objectives and spatial scales. HySPAR was part of a three

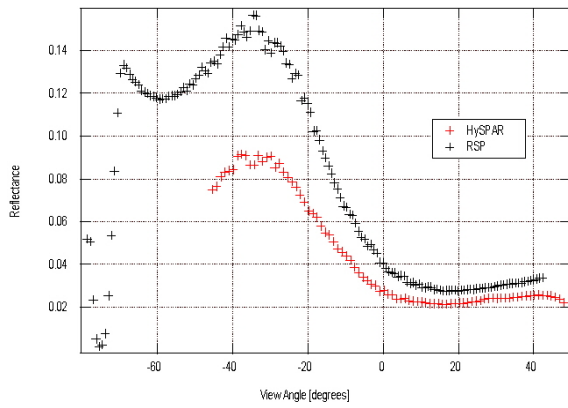


Fig. 4. Comparison of HySPAR and RSP principal plane unpolarized reflectance data over the Gulf of Mexico. The lower reflectance values obtained by HySPAR appear to be due to a sensor pointing error rather than radiometric calibration accuracy (see text). The wavelength is 670 nm and the bandwidths are 36 nm and 20 nm for HySPAR and RSP, respectively.

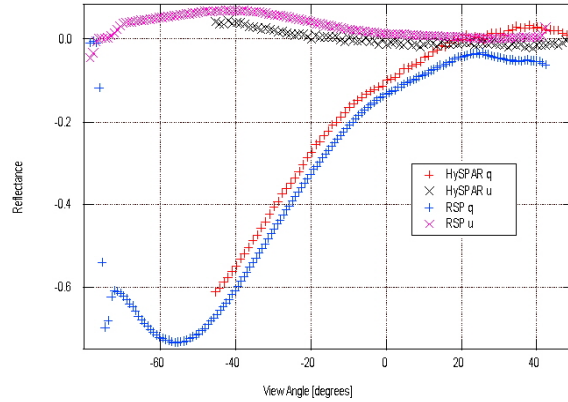


Fig. 5. Comparison of HySPAR and RSP principal plane linearly polarized reflectances over the Gulf of Mexico. The wavelength is 670 nm and the bandwidths are 36 nm and 20 nm for HySPAR and RSP, respectively.

sensor suite that included the High Spectral Resolution Lidar (HSRL) and the Langley A-Band Spectrometer (LAABS). These sensors flew on a King Air aircraft and participated in the Megacity Aerosol Experiment (MAX-Mex) that focused on the transport, transformation, and chemical and optical properties of aerosols. The King Air made a total of 15 flights during the campaign. RSP flew on a J31 aircraft and participated in the Intercontinental Chemical Transport Experiment-B (INTEX-B). Four flights were made during which the King Air and J31 executed coordinated flight segments to allow data comparison between HySPAR and RSP. Both HySPAR and RSP produce line images and are oriented in their respective aircraft such that the image is along track. Figure 4 shows the unpolarized reflectances measured by HySPAR and RSP during a coordinated measurement over the Gulf of Mexico (Lat/Lon: N21.52, W96.24). The HySPAR reflectance was computed from the intensity I using $\rho = \pi I / (\mu_0 F_0)$, where μ_0 is the cosine of the solar zenith angle and F_0 is the top of the atmosphere solar irradiance. For the 670 nm data, F_0 was taken to be $145.6 \text{ mW/cm}^2/\text{sr}/\mu\text{m}$. The King Air and J31 aircraft were flying at altitudes of 9000 meters and 4500 meters, respectively. We believe the discrepancy in the HySPAR data is due to a cross-track pointing error, causing HySPAR to image off the principal plane. This hypothesis is further supported by the cross principal plane data which shows reflectance data indicating that HySPAR is pointing closer to the solar glitter pattern than at nadir, as intended.

Figure 5 shows the normalized polarized reflectances measured by HySPAR and RSP. These reflectances, q and i , correspond to the Stokes vector Q and U components and are normalized by the total intensity (i.e., $q = Q/I$ and $u = U/I$). The polarized reflectances are less sensitive to the cross-track pointing error than is the total reflectance. It should be noted that, in addition to the instrument pointing error, the aircraft had a 13° difference in heading. Further, while RSP views through an open port, HySPAR must view through a window due to pressurized cabin of the King Air. The Fresnel transmittance of the window has not been removed from the

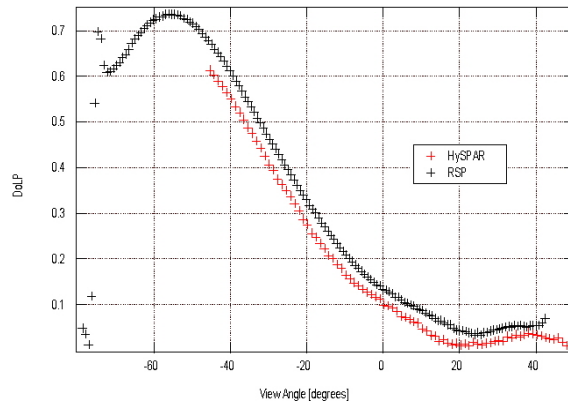


Fig. 6. Comparison of HySPAR and RSP principal plane degree of linear polarization data over the Gulf of Mexico. The wavelength is 670 nm and the bandwidths are 36 nm and 20 nm for HySPAR and RSP, respectively.

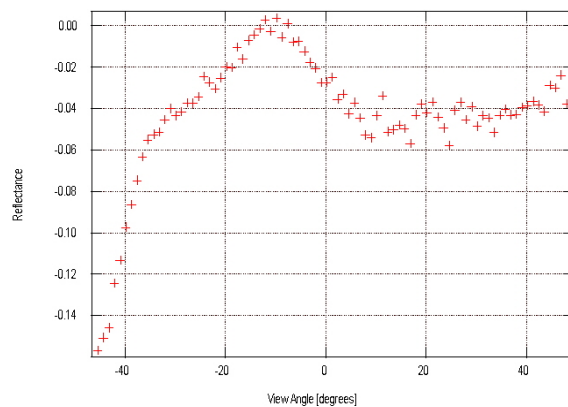


Fig. 7. HySPAR principal plane Stokes v component (V/I). The wavelength is 670 nm and the bandwidth is 36 nm.

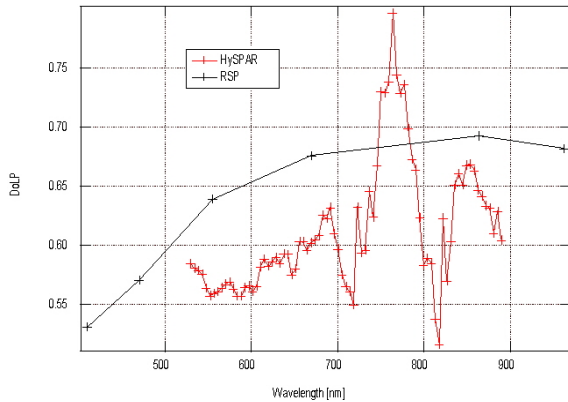


Fig. 8. Comparison of spectral DoLP measured by HySPAR and RSP in the backward direction, -45 degrees from nadir.

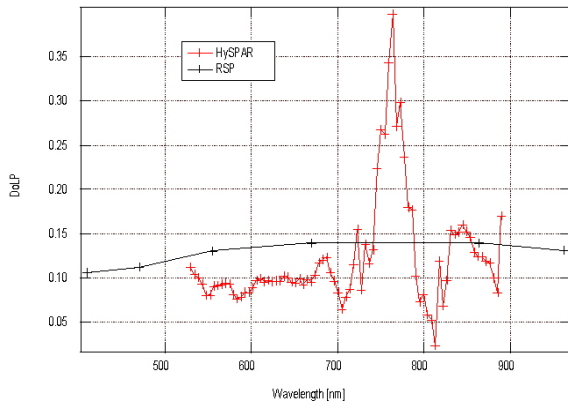


Fig. 9. Comparison of spectral DoLP measured by HySPAR and RSP at nadir.

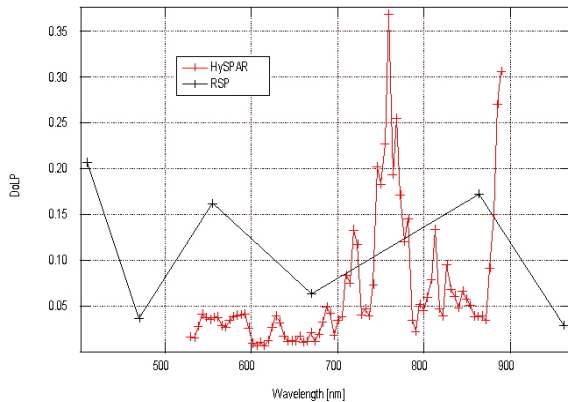


Fig. 10. Comparison of spectral DoLP measured by HySPAR and RSP in the forward direction, 45 degrees from nadir.

HySPAR data shown here. Because the window experiences approximately 1 atmosphere of pressure, it is necessary to carefully design the window and its supporting structure to avoid stress induced birefringence that would be very difficult to remove from the data. Figure 6 shows the degree of linear polarization (DoLP) computed as $\sqrt{q^2 + u^2}$. The noise equivalent degree of linear polarization (NeDoLP), as measured by the standard deviation of a detrended segment of the DoLP, is 0.0016 for this data in the region of the strongest signal. This approximately corresponds to the reciprocal of the shot noise dominated signal to noise ratio at this angle and wavelength.

Figure 7 shows the 670 nm v Stokes component ($v = V/I$). To the best of our knowledge, v Stokes component measurements such as this have not previously been made. It is not yet clear whether this data represents a natural effect, an aircraft window effect (possibly stress), or an artifact of the inversion algorithm.

Figures 8 through 10 show a comparison of spectral DoLP measured by the two sensors. In most cases, HySPAR measures a lower DoLP which, at least in part, is likely due to the pointing errors. The large feature in the HySPAR data centered around 760 nm is an artifact due to the spectral character in the oxygen A-band. As described previously, the HySPAR inversion algorithm is based on a model that assumes there is only linear spectral variation over the analysis band and this is clearly not true in the vicinity of the oxygen A-band. Accounting for such features using higher order components in the model would seem to be a straightforward extension of the inversion algorithm but this has not been implemented yet.

IV. CONCLUSION

Preliminary inspection of HySPAR data from its initial flight testing on the MILAGRO Campaign show reasonably good agreement with the validated RSP instrument. Unfortunately, due to what appear to be significant pointing errors on HySPAR, it is difficult to make a definitive comparison between the two instruments from this data alone. Measurement of the actual pointing error may allow us to make better comparisons. HySPAR measures significant amounts of circular polarization which does not resemble processing artifact. It remains to be determined whether this is due to window birefringence, a real atmospheric effect, or a processing artifact with which we are not familiar. The data presented here represent a small fraction of the HySPAR/RSP coordinated flight paths and a much smaller fraction of the total amount of MILAGRO data collected by HySPAR. Further analysis of the data is warranted to improve the validation of HySPAR as a viable sensor for airborne and, potentially, spaceborne aerosol retrievals.

ACKNOWLEDGMENT

HySPAR was developed under NASA/LARC contract NAS1-02115 and the MILAGRO measurements were conducted under NASA/GSFC (ESTO) contract NNG05HZ61C.

REFERENCES

- [1] Committee on Global Change Research, *Global Environmental Change: Research Pathways for the Next Decade*. National Academy Press, 1999. National Research Council.

- [2] J. Chowdhary, B. Cairns, M. Mishchenko, and L. Travis, "Retrieval of aerosol properties over the ocean using multispectral and multiangle photopolarimetric measurements from the Research Scanning Polarimeter," *Geophysical Research Letters*, vol. 28, no. 2, pp. 243–246, 2001.
- [3] M. Mishchenko and L. Travis, "Satellite retrieval of aerosol properties over the ocean using polarization as well as intensity of reflected sunlight," *Journal of Geophysical Research*, vol. 102, no. D14, pp. 16989–17013, 1997.
- [4] S. H. Jones, F. J. Iannarilli, and P. L. Kebabian, "Realization of quantitative-grade fieldable snapshot imaging spectropolarimeter," *Optics Express*, vol. 12, pp. 6559–6573, 2004.
- [5] B. Cairns, L. D. Travis, and E. E. Russell, "Research Scanning Polarimeter: calibration and ground-based measurements," *Proc. SPIE*, vol. 3754, pp. 186–197, 1999.
- [6] Collett, *Polarized Light*. Marcel Dekker, 1993.